Field-induced spin reorientation in $[Fe/Cr]_n$ multilayers studied by nuclear resonance reflectivity

M. Andreeva,[1,*] A. Gupta,[2] G. Sharma,[2,3] S. Kamali,[4] K. Okada,[5] and Y. Yoda[5]
[1]*Faculty of Physics, M. V. Lomonosov Moscow State University, Moscow 119991, Russia*
[2]*Center for Spintronic Materials, Amity University UP, Noida 201313, India*
[3]*Indore Center, UGC-DAE Consortium for Scientific Research, Indore 452017, India*
[4]*Department of Mechanical, Aerospace and Biomedical Engineering, University of Tennessee Space Institute, Tullahoma, Tennessee 37388, USA*
[5]*Japan Synchrotron Radiation Research Institute, SPring-8, Sayo, Hyogo 679-5198, Japan*
(Received 28 April 2015; published 5 October 2015)

We present depth-resolved nuclear resonance reflectivity studies of the magnetization evolution in $[^{57}Fe(3\,nm)/Cr\,(1.2\,nm)]_{10}$ multilayer under applied external field. The measurements have been performed at the station BL09XU of SPring-8 at different values of the external field (0–1500 Oe). We apply the joint fit of the delayed reflectivity curves and the time spectra of the nuclear resonance reflectivity measured at different grazing angles for enhancement of the depth resolution and reliability of results. We show that the azimuth angle, which is used in all papers devoted to the magnetization profile determination, has a more complicated physical sense due to the partially coherent averaging of the scattering amplitudes from magnetic lateral domains. We describe how to select the true azimuth angle from the determined "effective azimuth angle." Finally we obtain the noncollinear twisted magnetization depth profiles where the spin-flop state appears sequentially in different ^{57}Fe layers at increasing applied field.

DOI: 10.1103/PhysRevB.92.134403 PACS number(s): 75.25.−j, 42.25.Gy, 76.80.+y

I. INTRODUCTION

The interest in antiferromagnet/ferromagnet [AF/F] multilayers (MLs) started long ago, after the discovery of the Giant magnetoresistance (GMR) effect in [Fe/Cr] structures [1]. The immediately developed applications of this effect in microelectronics stimulated the extensive investigations of such systems resulting in the Nobel prize for Fert and Grünberg [2]. However, up to now some behavior features of AF/F multilayers at the action of the applied fields have not been investigated properly. The ladder-step magnetization curve, observed in [3] for $[Fe/Cr]_n$ multilayer, gives the authors the idea that the transition from the antiferromagnetic interlayer alignment to the ferromagnetic one under the action of the external field in such systems takes place as a layer-by-layer change of the sign of the magnetization. A similar model of the magnetization reorientation had been presented in the earlier paper [4]. Resembling sequential overturn of magnetization of ferromagnetic layers separated by nonmagnetic one was observed in a three-layer system by x-ray resonant magnetic scattering (XRMS) [5]. Polarized neutron reflectivity (PNR) and off-specular scattering was measured at the Institute Laue Langevin on the reflectometer ADAM from the sample $[Cr\,(0.9\,nm)/^{57}Fe(6.7\,nm)]_{12}$ of (100) orientation in the external magnetic field of 19.5 mT applied along an in-plane easy axis (001) after saturation in a field of 1 T. The data gave experimental evidence of the nonuniform twisted canted state in the spin-flop phase [6]. The canting angles are maximal in the end layers and progressively relax towards the middle of the ML from both sides. The presence of magnetic off-specular scattering (vanishing at saturation) observed in this experiment meant that the layer magnetization was laterally not homogeneous, but rather decomposed into domains. A visualization of the field evolution of the $[Fe(1.4\,nm)/Cr(1.1\,nm)]_{20}$ magnetic structure grown with a (211) orientation was obtained by the least-squares fitting of the PNR data [7]. The authors concluded that the obtained picture quite well reproduced the theoretical predictions of [8–10]; in particular it was shown that the spin-flopped region started from the top layer and was moved toward the center of the superlattice resulting in two antiphase domains. The similar complicated picture of the magnetization reorientation under the applied field was tested by a PNR experiment in [11] for a $[Fe(4\,nm)/Cr\,(1.1\,nm)]_{22}$ superlattice with cubic crystalline anisotropy. Measurements were performed under the applied fields 600, 200, 60, and 30 mT in order to probe the magnetization depth profile. The finding of the authors based on the data fit was that they got proof of the predicted picture of the magnetization reorientation in decreasing fields.

The theories so far developed [8–14] present a rather complicated picture of the layer-by-layer reorientation in the antiferromagnetic MLs under the applied field. However, in some papers the evolution of the layer magnetization vectors is treated with the assumption that magnetizations in all even and in all odd magnetic layers are collinear; in other words the reorientation of each magnetic sublattice takes place cophased. So the process of reorientation under the external field could be described just by two azimuth angles: each one for separate magnetic sublattice. In [15] this model was used for the description of the hysteresis loops measured by the intensity variation of the half-order Bragg peak at the reflection of the soft π linear-polarized x rays (at the L_3 edge of Fe) from $[Fe(1.52\,nm)/Cr\,(2.56\,nm)]_{10}$ ML. In [16] the variation of the layer magnetization directions in [Fe/FeO] superstructure was studied by nuclear resonance reflectivity (NRR) under gradual increase of the external field. The results were interpreted by an almost orthogonal moment alignment between adjacent Fe layers that are progressively rotated and finally collapsed to the direction of the applied filed. The result was later tested by PNR measurements [17].

*Mandreeva1@yandex.ru

In our paper we have performed a thorough investigation of the $[^{57}\mathrm{Fe}\,(3.0\,\mathrm{nm})/\mathrm{Cr}\,(1.2\,\mathrm{nm})]_{10}$ multilayer with antiferromagnetic interlayer coupling by means of the NRR using gradual increase of the external field. We have used the basic advantage of NRR experiments supplying the possibility to measure the time spectra of reflectivity at selected angles of incidence in addition to the NRR angular reflectivity curve. In such a way we got the combination of the spectroscopic and diffraction information in one experiment that supplies us with depth-profile information about hyperfine interactions in ^{57}Fe layers and their magnetization direction. The joint fit of the angular curve and the time spectra of reflectivity, measured at several grazing angles, adds reliability to the obtained magnetization depth profiles.

We have made as well the essential correction to the previous ways of the data interpretation taking into account the partially coherent averaging of the reflected amplitudes from magnetic lateral domains. In this way we have been able to explain the results, obtained in two geometries: for transverse (T geometry) and longitudinal (L geometry) direction of the applied field relative synchrotron radiation (SR) beam.

II. THEORY

Up to the present time the NRR experiments at synchrotron beamlines have been performed in the time domain: The short pulse of synchrotron radiation (SR) excites all hyperfine transitions in the resonant nuclei simultaneously and γ-quanta, attendant to the decay of the excited states, are measured as a function of the delay time after a prompt SR pulse (nowadays with the developing of the nuclear monochromators it is possible to measure the spectra of reflectivity in the energy scale as common Mössbauer spectra [18–20]).

The time spectra of reflectivity $I(\theta,t)$ are calculated by applying the Fourier transform to the energy dependent σ- and π-reflectivity amplitudes.

$$I(\theta,t) = \left|\frac{1}{2\pi}\int_{-\infty}^{+\infty} R^{\pi\Rightarrow\sigma}(\theta,\omega)e^{-i\omega t}d\omega\right|^2 + \left|\frac{1}{2\pi}\int_{-\infty}^{+\infty} R^{\pi\Rightarrow\pi}(\theta,\omega)e^{-i\omega t}d\omega\right|^2. \quad (1)$$

Here we suppose that the incident SR field is σ polarized, but the Mössbauer transition in ^{57}Fe is of the magnetic dipole $M1$ type, so we follow the magnetic field of the radiation with the nuclei, which is π polarized. Hyperfine interactions reveal themselves in the time spectra of reflectivity by the quantum beats well described for the nuclear resonance forward scattering, but the data interpretation is complicated by the dynamical beats and other effects specific for coherent decay of the excited nuclear system [21]. The time spectra of NRR are also distorted by the dynamical effects but, more essentially, by the phase relations between waves scattered by different layers. This last circumstance does not exist for the forward scattering and it provides us with the depth selective information relative to the investigated parameters. The selectivity of the spectra measured at the different Bragg maxima to the depth distribution of hyperfine fields over one repetition period have been presented in [22] and thoroughly analyzed in [23]. In our case we are mostly interested in the magnetization profile in the whole ML.

The delayed nuclear reflectivity curve $I^{\mathrm{delayed}}(\theta)$ is calculated by the integration of the time spectra over the whole delay time after the prompt SR pulse,

$$I^{\mathrm{delayed}}(\theta) = \int_{\Delta}^{T} I(\theta t)dt, \quad (2)$$

where Δ is the dead time of the APD detector and T is the time interval between the successive SR pulses. Note that the actual value of Δ can essentially distort the behavior of $I^{\mathrm{delayed}}(\theta)$ [24]. Normally the nuclear decay is virtually finished during the interval T; however, if this interval is comparable with the lifetime of the excited nuclear state then the "tail" of the reflectivity decay from the previous pulse should be added to (2).

For the NRR data treatment we used our computer package REFTIM [25,26]. The reflectivity theory used in calculations is described in [27]. For the case of complicated noncollinear magnetic MLs we should work with the reflectivity matrices taking into account the possible polarization change of the radiation during multiple reflections transitions through layer boundaries. Such matrix formalism has been developed in optics [28,29], and it has been adjusted for the case of very small grazing angles used in reflectivity measurements with Mössbauer radiation in [30–32].

The calculations of the nuclear resonance reflectivity for the experimental data fit have been performed by the exact formula, presented in [27]; however, in order to unveil some important restrictions of the conventional data interpretation we simplify the theory. For the angles much larger than the critical angle of the total external reflection the reflectivity can be described in the kinematical limit of the exact theory. For the scalar susceptibility of layers it has been accurately derived in [33] and for the case of anisotropic layers it is done in [34]:

$$\hat{R} \cong \sum_{j=1}^{L} e^{-i\frac{\omega}{c}d_1\hat{n}_1^-}\cdots e^{-i\frac{\omega}{c}d_{j-1}1\hat{n}_{j-1}^-}\hat{r}_{j-1,j} \times e^{+i\frac{\omega}{c}d_{j-1}\hat{n}_{j-1}^+}\cdots e^{+i\frac{\omega}{c}d_1\hat{n}_1^+}. \quad (3)$$

Here $\hat{r}_{j-1,j}$ represents the one-time reflectivity matrices at the $(j-1)/j$ boundary and $\hat{n}_j^{\pm}$ is the refraction matrix for the waves in the direct and reverse directions (similar to ones used in the early work devoted to the Faraday rotation for Mössbauer radiation [35], but for inclined geometry). For these matrices the following expressions take place:

$$\hat{r}_{j-1,j} = \frac{1}{4\sin^2\theta}\left(\hat{\chi}_{j-1}^{\perp} - \hat{\chi}_j^{\perp}\right), \quad \hat{n}_j^{\pm} = \pm\left(\sin\theta + \frac{\hat{\chi}_j^{\pm\perp}}{2\sin\theta}\right). \quad (4)$$

For small grazing angles typically used in NRR experiments the transversal 2×2 matrices $\hat{\chi}_j^{\perp}$ in (4) can be calculated in the plane perpendicular to the beam direction $\vec{k}_o$,

$$\hat{\chi}_j^{\perp} = \frac{\lambda^2}{\pi}\rho\hat{f}_{\vec{k}_o\to\vec{k}_o}. \quad (5)$$

This is the known relation between the susceptibility tensor and the coherent forward scattering amplitude $\hat{f}_{\vec{k}_o\to\vec{k}_o}$, where ρ is the volume density of the scattering centers.

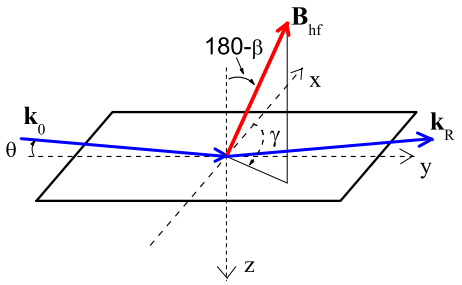

FIG. 1. (Color online) The used coordinate system.

Unfortunately, in the general case the matrix exponentials $e^{i\hat{n}kz}$ in (3) cannot be rearranged, so this kinematical method of computation does not considerably speed up the computations. Only if the polarization-dependent absorption can be neglected, the expression (3) can be simplified to the following expression (formally similar to that obtained in [33], but with matrices $\hat{\chi}_j^{\perp}$):

$$\hat{R} \cong \frac{1}{4\sin^2\theta} \sum_{j=1}^{N} e^{iQz_{j-1}} \left(\hat{\chi}_{j-1}^{\perp} - \hat{\chi}_j^{\perp}\right), \tag{6}$$

where $Q = \frac{4\pi}{\lambda} \sin\theta$ is the scattering vector and z_{j-1} is the z coordinate of the $(j-1)/j$ boundary counting from the surface; N is the number of the interlayer boundaries. Proceeding from this simplest expression (6) for the reflectivity amplitude, NRR experiments are often referred to as the forward scattering experiments. However, the different phases [$e^{i\,Q\,z_{j-1}}$ in (6)] lead to much more complicated shape of the reflectivity spectra than of the forward scattering spectra. At the same time these phases supply us with the depth resolution. The kinematical approach is not applicable near the critical angle; however, the kinematical formula (6) gives us an opportunity for qualitative considerations of some effects.

If we define the $\vec{B}_{hf}$ orientation by the polar β and azimuth γ angles (see Fig. 1), the matrix $\hat{\chi}_j^{\perp}$ in (6) in the σ, π unit vectors for different hyperfine transitions takes the form (see Supplemental Material [27])

$$\hat{\chi}^{\perp}_{\Delta m=0} \propto \begin{pmatrix} \sin^2\beta\cos^2\gamma & -\sin\beta\cos\beta\cos\gamma \\ -\sin\beta\cos\beta\cos\gamma & \cos^2\beta \end{pmatrix}, \tag{7}$$

$$\hat{\chi}^{\perp}_{\Delta m=\pm 1} \propto \frac{1}{2}\begin{pmatrix} \sin^2\gamma + \cos^2\gamma\cos^2\beta & (\cos\beta\cos\gamma \mp i\sin\gamma)\sin\beta \\ (\cos\beta\cos\gamma \pm i\sin\gamma)\sin\beta & \sin^2\beta \end{pmatrix}. \tag{8}$$

We point out some features of the angular dependence of the scattering matrices in the case of the magnetic hyperfine splitting of the nuclear levels. For the scattering of the π-polarized radiation (that is, the polarization of the magnetic field of the σ-polarized SR) and in the case of $\beta = 90^\circ$ the transitions with $\Delta m = 0$ are not presented in the scattering spectrum, the amplitude of scattering at the $\Delta m = \pm 1$ transitions is not changed after substitution γ by $(180 - \gamma)$ (symmetrical relative the beam direction), and at the substitution γ by $(-\gamma)$ the scattering amplitude changes the sign of the scattering component of the changed polarization state. So this polarization state in the scattered amplitude provides the creation of the "magnetic maxima" on the nuclear resonance reflectivity curve for the multilayer with antiferromagnetic or noncollinear interlayer coupling.

Note that because $\hat{\chi}^{\rm nucl}(\omega)$ as well as χ^{el} in the multilayer is specific for each separate sublayer, the description of the multilayer model includes the huge number of independent parameters for fit: χ_n^{el}, $\rho_{n,j}^{\rm nucl}$, $B_{hf}^{(n,j)}$ (the magnetic hyperfine field value), $dB_{hf}^{(n,j)}$ (their distribution), $\Delta_{\rm EFG}^{(n,j)}$ (the electric quadrupole splitting), $IS_{n,j}$ (the isomeric shift), $\Delta G_{n,j}$ (the hyperfine line broadenings), and $\beta_{n,j}$, $\gamma_{n,j}$ or to the possible portion of the random or plane orientation in each $n = 1, \ldots, N$ sublayer characterizing by $j = 1, \ldots, J$ hyperfine multiplets.

The huge number of parameters for fit causes the necessity to fit simultaneously all available experimental data: conversion electron Mössbauer spectrum (CEMS), measured at normal incidence, x-ray reflectivity curve, nuclear resonance reflectivity curve, and the set of nuclear resonance spectra, measured at different grazing angles.

III. PARTIAL TRANSVERSE COHERENCE OF THE INCIDENT BEAM

The most nontrivial description for the reflectivity is needed for the case when lateral inhomogeneous magnetic structure takes place. Nowadays it is clear that even a very thin magnetic ML has lateral domains. A lot of experimental methods successfully visualize them. Up to now most of the papers devoted to the NRR experiments (excluding the off-specular measurements, in, e.g., [36]) have presented the definite azimuth magnetization angle for each sublayer as the result of the reflectivity data fit [16,37–39]. If the measurements are not performed in the saturation state of the sample, then it would be in contradiction with the latest results on the domain structure visualizations for ultrathin multilayers (see, e.g., [40–42]).

NRR measurements are executed at grazing angles $\sim 10^{-3}$ rad. Even the very narrow SR beam ($\sim 20\,\mu$m) illuminates a rather large area on the surface $\sim 20\,000\,\mu$m (along the beam direction) which exceeds the typical lateral domain size. If in the absence of the external field we have an equal number of domains with different orientation of $\vec{B}_{hf}$ in the surface plane, we could suppose that we have the case of the random orientation of the hyperfine fields in the surface plane ($\beta = 90^\circ$), which for a σ-polarized SR beam gives the identical results with the case $\beta = 90^\circ$, $\gamma = 0^\circ$, and 180° [43–45] (see also [27]). But surprisingly the NRR

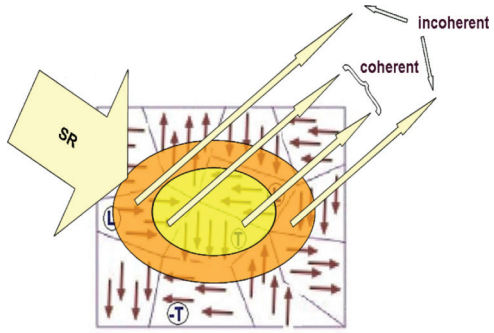

FIG. 2. (Color online) The illustration of the partially coherent interference of waves reflected by different domains.

data interpretation has given the definite azimuth angle for the magnetization direction which is difficult to explain, especially for the polycrystalline film in, e.g., [37].

Here we try to give a more realistic interpretation of the results. It takes into account the finite transverse coherence length of SR [46,47]. We should suppose that probably not all scattered amplitudes from different domains are added coherently in the reflectivity signal (Fig. 2).

Assuming the fourfold in-plane anisotropy we will operate with four possible σ- and π-polarized reflected amplitudes $f_{\sigma,\pi}^{L,-L,T,-T}$ for domains with magnetization directions along the beam (L and $-L$) and perpendicular to the beam (T and $-T$). So Therefore the reflectivity intensity can be presented by the formula

$$\begin{aligned} I_R(t) \propto & \left[\left|\alpha f_\pi^L\right|^2 + \left|\beta f_\pi^{-L}\right|^2 + \left|\gamma f_\pi^T\right|^2 + \left|\delta f_\pi^{-T}\right|^2\right. \\ & \left. +2C_{\rm coh}{\rm Re}\left(\alpha\beta f_\pi^L f_\pi^{-L^*} + \alpha\gamma f_\pi^L f_\pi^{T*} + \alpha\delta f_\pi^L f_\pi^{-T^*} + \beta\gamma f_\pi^{-L} f_\pi^{T^*} + \beta\delta f_\pi^{-L} f_\pi^{-T^*} + \gamma\delta f_\pi^T f_\pi^{-T^*}\right)\right] \\ & +\left[\left|\alpha f_\sigma^L\right|^2 + \left|\beta f_\sigma^{-L}\right|^2 + \left|\gamma f_\sigma^T\right|^2 + \left|\delta f_\sigma^{-T}\right|^2 + 2C_{\rm coh}{\rm Re}(\alpha\beta f_\sigma^L f_\sigma^{-L^*} + \alpha\gamma f_\sigma^L f_\sigma^{T^*} + \alpha\delta f_\sigma^L f_\sigma^{-T^*}\right. \\ & \left. +\beta\gamma f_\sigma^{-L} f_\sigma^{T^*} + \beta\delta f_\sigma^{-L} f_\sigma^{-T^*} + \gamma\delta f_\sigma^T f_\sigma^{-T^*})\right], \end{aligned} \tag{9}$$

where $\alpha,\beta,\gamma,\delta$ are the relative amount of the L, $-L$, T, $-T$ domains, respectively. In (9) we insert the factor $C_{\rm coh}$ ($0 \leqslant C_{\rm coh} \leqslant 1$) which supplies the suppression of the interference of the waves reflected by different domains due to the partial coherence of the incident SR beam. Following the consideration in [47] we can write

$$C_{\rm coh} = \exp\left[-\tfrac{1}{2}(D_{\rm domains}/\xi_t)^2\right], \tag{10}$$

where ξ_t is the transverse coherence length of the SR beam, and $D_{\rm domains}$ is the characteristic lateral domain size. If $D_{\rm domains} \gg \xi_t$, $C_{\rm coh} \approx 0$, the interference between scattering waves from different domains is absent. If $D_{\rm domains} \ll \xi_t$, $C_{\rm coh} \approx 1$ and scattering from the whole surface is fully coherent.

When $\vec{B}_{hf}$ is orientated in the surface plane, it can be shown that in the kinematical approximation (remember that we consider $M1$ transition, so we have a π-polarized SR beam with respect to the magnetic field of radiation),

$$f_\pi^L = f_\pi^{-L} = f_\pi^T = f_\pi^{-T} = f_\pi(t), \tag{11}$$

$$f_\sigma^L = -f_\sigma^{-L} = f_\sigma(t); \quad f_\sigma^T = f_\sigma^{-T} = 0. \tag{12}$$

So in the fully coherent scattering ($C_{\rm coh} = 1$),

$$I_R(t) \propto [(\alpha+\beta+\gamma+\delta)^2 |f_\pi(t)|^2 + (\alpha-\beta)^2 |f_\sigma(t)|^2], \tag{13}$$

and when $\alpha = \beta = \gamma = \delta = 1$, no contribution of $|f_\sigma(t)|^2$ will be inserted to the time spectrum of reflectivity $I_R(t) \propto |f_\pi(t)|^2$. In the case of completely incoherent scattering ($C_{\rm coh} = 0$),

$$I_R(t) \propto [(\alpha^2+\beta^2+\gamma^2+\delta^2)|f_\pi(t)|^2 + (\alpha^2+\beta^2)|f_\sigma(t)|^2], \tag{14}$$

and when $\alpha = \beta = \gamma = \delta = 1$, we have $I_R(t) = A[|f_\pi(t)|^2 + \frac{1}{2}|f_\sigma(t)|^2]$. In general for any value of $C_{\rm coh}$ we have

$$I_R(t) \propto (1+3C_{\rm coh})\left|f_\pi(t)\right|^2 + \tfrac{1}{2}(1-C_{\rm coh})\left|f_\sigma(t)\right|^2. \tag{15}$$

We can get the same mixture of $|f_\pi(t)|^2$ and $|f_\sigma(t)|^2$ dependencies in the case of the homogeneous magnetization direction with definite azimuth angle $\gamma^{\rm eff}$ for $\vec{B}_{hf}$ orientation:

$$I_R(t) \propto |f_\pi(t)|^2 + \sin^2\gamma^{\rm eff}|f_\sigma(t)|^2. \tag{16}$$

Comparing (15) with (16) we can claim that the interpretation of the time spectra of reflectivity, presented in many papers in terms of uniaxial anisotropy of the sample magnetization (single-domain state), can in reality be masked by the multidomain state due to the restricted coherence length of radiation. For any effective azimuth angle $\gamma^{\rm eff}$, obtained by the fit of the reflectivity time spectrum, measured at one sample orientation, we can give a fully adequate description with some value of the partial coherence parameter $C_{\rm coh}$ according to the equation for $C_{\rm coh}$,

$$\frac{(1-C_{\rm coh})}{2\,(1+3\,C_{\rm coh})} = \sin^2\gamma^{\rm eff}. \tag{17}$$

In many cases the choice between the two different descriptions of the data can be made with the sample rotation, say at 90°. If for the new spectrum interpretation you change the azimuth angle in the model, also for 90°, you deal with the single-domain state with definite magnetization direction. If you do not change anything in the model, then it is proof of the partial coherence of the scattered waves from different domains. In the case of the external field application we should not rotate the sample but should change the direction of the external field; however, in practice such comparison is not trivial, because the sample magnetization always depends on the prehistory and you can get another magnetization state in the process of increasing or decreasing of the external field.

Strictly speaking the lateral inhomogeneity always leads to the diffuse scattering. The "magnetic" diffuse scattering (or small-angle scattering in the case of forward scattering), brightly demonstrated for nuclear resonance scattering (NRS) in [48,49], gives the more direct information about the lateral magnetic domain size. However, the theory of the diffuse scattering, especially for the case of the spectral inhomogeneity, is rather complicated (see, e.g., [50,51]) and needs the use of the correlation functions for the description of the lateral distribution of the inhomogeneities, while for specular reflectivity this factor is absent and just the partial transverse coherence of the synchrotron beam is actual. Diffuse NRS experiments are rather difficult to do (in the allocated beam time) and the resulting advantage would have been of limited use for determination of the depth profiles of magnetization direction. In our work we use just the specular NRR reflectivity and present the simplest and clearest description of the influence of the finite transverse coherence of the synchrotron beam on the NRR from multidomain multilayers. Note that similar simplification for description of the specular reflectivity from rough surfaces, like a simple exponential factor, decreasing the Fresnel amplitude of specular reflectivity, is commonly used for the x-ray reflectivity data treatment.

It is interesting that the surface domain influence on the specular NRR reflectivity destroys the common opinion that the specular reflectivity provides information on the depth profiles only, while off-specular scattering does so on the lateral structure of scattering layers. The same idea has been presented in [51], where the authors have shown that the lateral domain occurrence leads to the decrease of the "antiferromagnetic maximum" on the delayed specular NRR curve. However, in the NRR theory the authors of [51] have used a rather general parameter: "a specific magnetic bias parameter η" (Eq. (45) in [51]), which is a part of the magnetization along the field direction. In addition it has been assumed a strict antiferromagnetic interlayer coupling. Therefore their approach would be helpless in the description of the twisted magnetization profiles.

IV. EXPERIMENT

The experiment was performed at station BL09XU of SPring-8. The angular dependencies and the time spectra of the NRR were measured at each step of the gradually increasing external field from 0 up to 1500 Oe in L and T geometries. For such measurements the special design of the magnet had been created.

The ^{57}Fe (2.0 nm)/Cr (1.2 nm)]$_{10}$, [^{57}Fe (2.0 nm/Cr (1.2 nm)]$_{20}$, and [^{57}Fe (3.0 nm)/Cr (1.2 nm)]$_{10}$ have been grown as samples for our investigation at Indore (India). Deposition on Si substrate was carried out using ion beam sputtering at room temperature in a UHV chamber with a base pressure of 1×10^{-7} mbar. Sputtering was done using a 3-cm broad Kaufman-type ion source with 1-keV Ar ions. Fe layers were prepared with 95% enriched ^{57}Fe target in order to enhance the NRR signal. Before the measurements at SPring-8 the conversion electron Mössbauer spectra (CEMS) were measured (Fig. 3) as well as the magnetization curves (Fig. 4). CEMS can be fitted with several magnetic subspectra (we manage to do that with three subspectra used for the subsequent fit of the time spectra; see Fig. 3). The ratio of the hyperfine lines confirms the plane anisotropy of the magnetization; i.e., all $\vec{B}_{hf}$ lay in the surface plane.

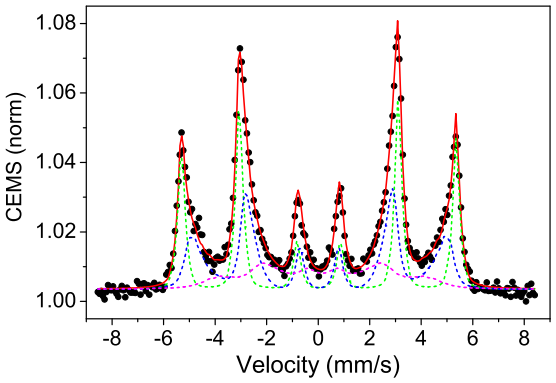

FIG. 3. (Color online) Experimental CEMS (dots) and fit result by three magnetic subspectra (dotted lines) corresponding to $\vec{B}_{hf}^{(1)} = 33.1$ T, $\vec{B}_{hf}^{(2)} = 30.8$ T, $\vec{B}_{hf}^{(3)} = 24.5$ T for the [^{57}Fe (3.0 nm)/Cr (1.2 nm)]$_{10}$ sample.

Magneto-optical Kerr effect (MOKE) measurements were done in longitudinal geometry using a He-Ne laser (632.8 nm wavelength), with a maximum magnetic field of 1500 Oe.

Magnetization measurements did not reveal the noticeable anisotropy in the surface plane. Just slight manifestation of the steplike behavior and weak hysteresis can be seen on the magnetization curves. The small values of these effects could be explained by the multidomain surface structure of our film.

The antiferromagnetic interlayer coupling of ^{57}Fe layers was evidently detected by the occurrence of the half-order Bragg peaks (Fig. 5) on the delayed reflectivity curves measured at SPring-8. We start these measurements with the sample [^{57}Fe (2.0 nm/Cr (1.2 nm)]$_{20}$ and follow the disappearance of these "magnetic peaks" during the external field increase in the longitudinal geometry. However, we needed also the time spectra of reflectivity, but at the field decrease we came to another magnetization state of the sample, so later we decided to investigate the whole set of data in the increasing field with another [^{57}Fe (3.0 nm)/Cr (1.2 nm)]$_{10}$ sample. For that sample we got the most complete set of data, which we present now.

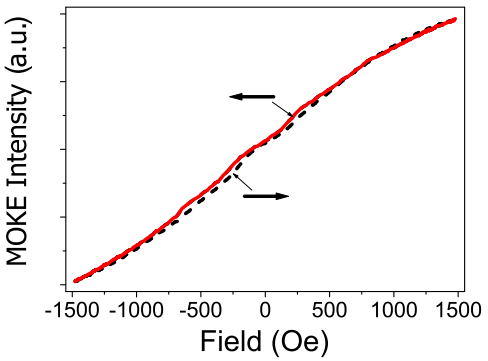

FIG. 4. (Color online) Magnetization curve for [^{57}Fe (3.0 nm)/Cr (1.2 nm)]$_{10}$ sample, measured by magneto-optical Kerr effect. The steps and small hysteresis are hardly seen.

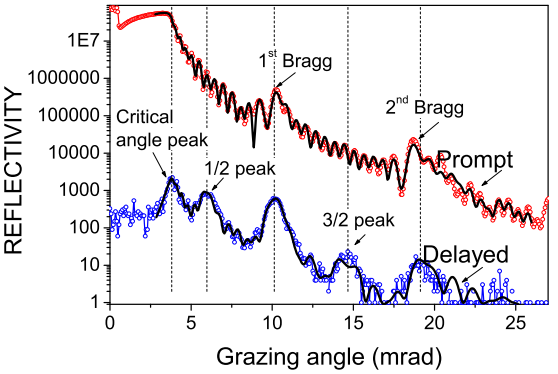

FIG. 5. (Color online) Prompt and delayed reflectivity measured without external field for the sample $[^{57}\text{Fe}\ (3.0\,\text{nm})/\text{Cr}\ (1.2\,\text{nm})]_{10}$. The angles at which the time spectra of the NRR were measured are marked by the dashed vertical lines.

The fit of the prompt reflectivity curve gives us the electron density profile (Fig. 6). It is not simple and we see that not only the top Cr layer but also the surface Fe/Cr bilayer and bilayer at the interface with Cr buffer layer are somehow distracted. The electron density of Fe and Cr layers differs from the standard values due to some intermixture. The larger than standard values of $\text{Im}\chi$ in the interfaces can be explained by the roughness-initiated diminution of radiation.

The fit of the delayed reflectivity curve should be done simultaneously with the fit of the time spectra of reflectivity which were measured at five angles: at the critical angle, at half-, first-, $\frac{3}{2}$-, and second-order Bragg peaks (Fig. 7). The shapes of the time spectra measured at the marked grazing angles are rather different; however, their Fourier transforms contain the same frequency beats and confirm that we have the plane orientation of $\vec{B}_{hf}$ when just the $\Delta m = \pm 1$ transitions are excited by the σ-polarized SR. The corresponding four lines in the conventional Mössbauer spectrum are shown in the inset of Fig. 7. The basic frequency beats originate from the interference of these hyperfine transitions (marked by vertical lines). At the same time the Fourier transform reveals the difference in the magnitude of these frequency beats. It has been shown that the first-order Bragg peak is mostly sensitive to the hyperfine fields in the center of the ^{57}Fe layers, but in the second-order Bragg peak the contribution from interfaces

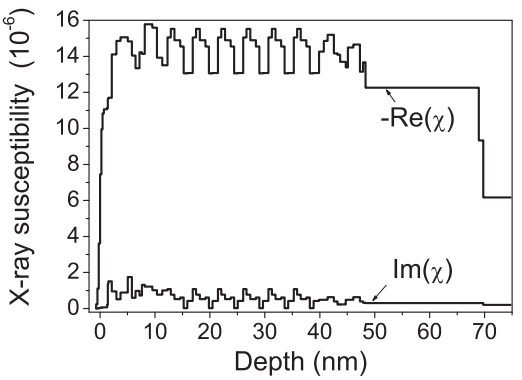

FIG. 6. Depth profile of the electron density and of the absorption obtained by the fit of the prompt reflectivity curves.

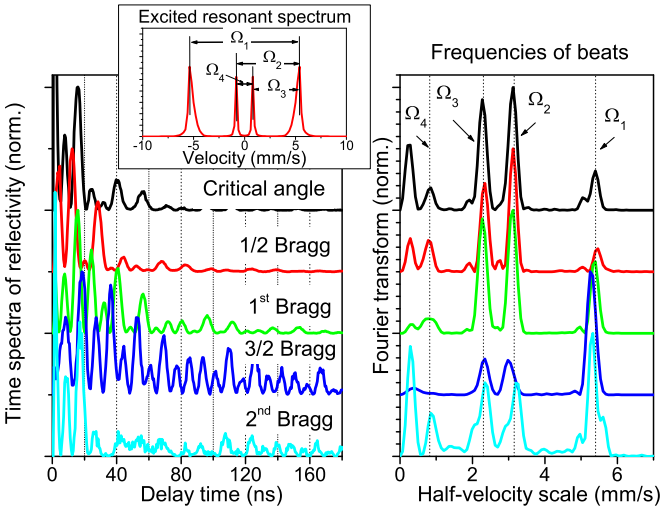

FIG. 7. (Color online) NRR time spectra, measured at the angles, marked by vertical lines in Fig. 5 (left panel), and their Fourier transform (right panel). The spectra are normalized and vertically shifted.

dominates [23]. So the essential increase of the amplitude of the largest frequency beat for the second-order Bragg peak can be explained by considerable disorientation of the B_{hf} in the interfaces compared with the center part of ^{57}Fe layers. The same deduction has been obtained by the fit of the NRR data for $[^{57}\text{Fe}/\text{Cr}]$ ML [37] and XRMR, PNR data for $[\text{Fe}(35\,\text{Å})/\text{Gd}\,(50\,\text{Å})]_5$ ML in [52].

For the joint fit of the delayed reflectivity and the time spectra of reflectivity we use the parameters obtained by the Mössbauer spectrum fit and prompt reflectivity curve fit. The main purpose of the joint fit is the depth distribution of the three chosen $\vec{B}_{hf}$ and their effective orientation in plane.

The fitted delayed curve and the time spectra of reflectivity in the case, when the external field is absent, are shown in Figs. 5 and 8. The obtained depth profiles for the three chosen hyperfine fields are presented in Fig. 9.

As we see in Fig. 9 the highest hyperfine field of 33.1 T is attributed to the nuclei situated preferably near the top interface. That means that the Fe-on-Cr interface is more diffused than the Cr-on Fe interface in our sample.

We expected that when the external field is absent the hyperfine fields, antiferromagnetically coupled between adjacent ^{57}Fe layers, have no preferable azimuth direction in the surface plane. Even if there is some uniaxial anisotropy in the multilayer due to internal stresses generated during deposition (as observed in [53]] for Finemet ferromagnetic alloy) *we cannot exclude* 180° *lateral domains. The coherent averaging of scattering amplitudes in that case should give the effective azimuth angle* 0°/180° for the magnetization direction in antiferromagnetic bilayers. However, the fit of our data set has been more or less successful with the azimuth angles of 20°/−160° (or equivalently −20°/160°). The influence of the partial coherence of the scattering from different domains, considered in the previous section, can explain this result. Using (17) for the effective azimuth angle $\gamma^{\text{eff}} = 20°$, we get $C_{\text{coh}} = 0.45$, or $D_{\text{domains}}/\xi_t = 1.26$. The value of the transverse coherence length for the European Synchrotron Radiation

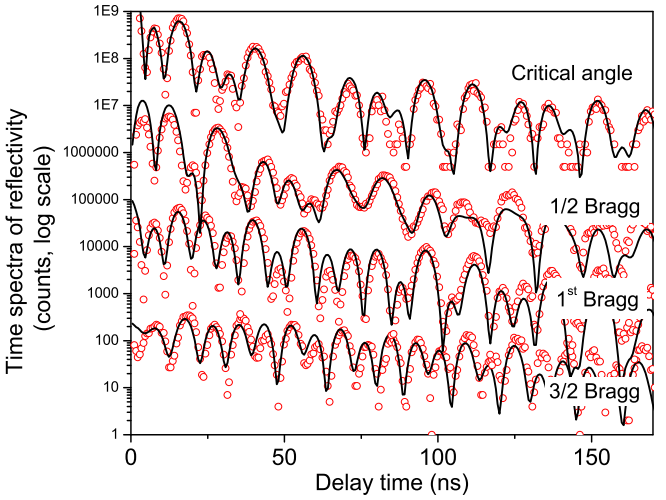

FIG. 8. (Color online) Time spectra of NRR measured at four grazing angles in logarithm scale and vertically shifted. Symbols represent the experimental data, lines—the fit results.

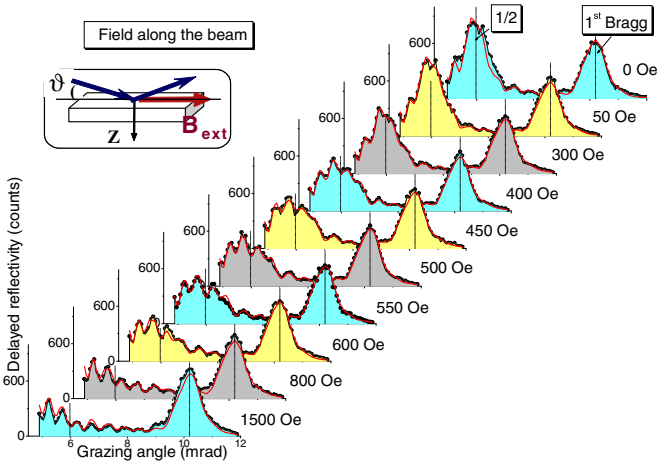

FIG. 10. (Color online) Delayed reflectivity curves measured at different magnitude of the ascending external field in L geometry. Symbols represent the experimental data, lines—the fit results.

Facility (ESRF) source has been measured as $\sim 3\,\mu$m in [46] (notice that it depends on the slit sizes); at a grazing angle ~ 10 mrad the lateral coherence length is $\xi_t \sim 300\,\mu$m, so $D_{\text{domains}} \sim 400\,\mu$m appears to be a quite true result. It is interesting that here we get the estimations of the average magnetic domain size directly from the nuclear resonance specular reflectivity data but not from the nuclear resonance diffuse scattering. It would be interesting in future to compare the obtained result with the domain visualization by direct methods or results of the diffuse scattering.

V. THE RESULTS OF THE EXTERNAL FIELD INFLUENCE

The results of the external field influence are presented in Figs. 10–15. In L geometry the relative intensity of the half-order Bragg peak compared with the first-order Bragg peak is decreased with the increase of the field magnitude; see Fig. 10. It could be interpreted by the gradual change of the antiferromagnetic interlayer alignment to the canted state as if the difference of the azimuth angles in the adjacent ^{57}Fe layers changes from 180° at zero field to 0° at 1500 Oe. However, the measurements in T geometry are not consistent with such interpretation: at 600 Oe we have the essential increase of the half-order Bragg peak. Such effect has been observed earlier [49] and it was interpreted by the reorientation of the antiferromagnetically coupled magnetizations to the perpendicular direction relative to the external field—that is, the bulk spin-flop transition. The same results have been presented in the interpretation of the PNR experiments (e.g., in [6,7]). For the case of the perpendicular orientation of the antiferromagnetically coupled ML we do not have any difference in the scattering amplitudes from the adjacent ^{57}Fe layers in the L geometry, but they have opposite sign in the T geometry. So at the half-order Bragg peak we have zero sum for L geometry and maximal sum for T geometry when these waves from the magnetic period are added with the π space phase shift.

Quantitative interpretation of the layer magnetization reorientation by the action of the applied field has been obtained by the joint fit of the delayed reflectivity curve (Figs. 11 and

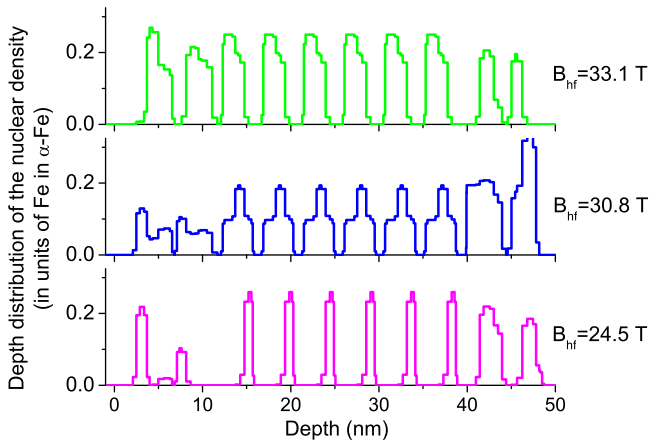

FIG. 9. (Color online) The depth distribution of the ^{57}Fe nuclei, characterizing by one of the three kinds of B_{hf}, obtained by the fit of CEM spectrum in Fig. 3.

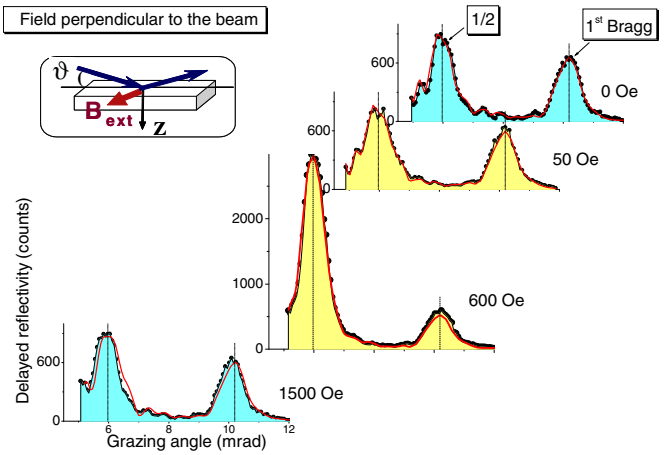

FIG. 11. (Color online) The same as in Fig. 10 but for T geometry.

12) and three time spectra (Figs. 12 and 13) measured for each value of the applied field. The final picture of the magnetization alignment for all used magnitudes of the applied field is given in Figs. 14 and 15.

At the first stage we supposed that in each magnetic sublattice (i.e., in the odd and even ^{57}Fe layers) collinear alignment in each of two magnetic sublevels takes place. This approximate result is presented in Fig. 14 by dashed vertical lines. It is significant to notice that in such approach we can get the more or less reasonable fit of the delayed reflectivity curves for all field magnitudes, but the obtained models do not reproduce all features of the experimental time spectra. For example, in Fig. 16 we compare the results for the half-order time spectra, measured under the applied 450-Oe field, obtained as the best joint fit of all the data for two models: the model of the collinear magnetization in each magnetic sublattice (dashed vertical lines in Fig. 14) and for the model, allowing the arbitrary magnetization direction in each ^{57}Fe layer. We see that the last, more complicated model gives a much better fit result, so we have used that model for all data.

Figures 14 and 15 present the very complicated picture of the change of the layer-by-layer change of the effective azimuth angle for magnetization directions in ^{57}Fe layers under the applied field. The most essential question now is how we can separate these effective angles into the effect of the partially coherent averaging over magnetic domains and the real picture of the magnetization directions.

That can be done by the comparison of the fit result, obtained in the L and T geometries. Unfortunately the measurements in T geometry have been done only at the selected field values (at 0, 50, 600, and 1500 Oe), and with another piece of the same sample in order to avoid the remanent magnetization effects after the first cycle of the magnetic field application (Figs. 11 and 13). The angular delayed curve and time spectra of reflectivity at zero external field are well fitted with the same hyperfine parameter and B_{hf} orientations ($20^\circ/-160^\circ$) which according to (41) we associate with $C_{\rm coh} = 0.45$.

At 50 Oe the fit results for two geometries are slightly different (Fig. 17). It is almost the same in the simplest model of the collinear magnetizations in each magnetic sublattice ($-9.6^\circ/147^\circ$—the effective angles prove to be connected with the SR direction, but not with the applied field direction), so it is the $C_{\rm coh}$ factor influence. The improved model shows the twisted layer-by-layer magnetizations which are closer to the external field for near-surface ^{57}Fe layers than moving off that direction and again slightly approaching that direction at the bottom layers. The marked twisted features are the same in both geometries, so this twisted part is connected with real change of the magnetization directions. However, the influence of the multidomain state is still predominant at 50 Oe, so the variations of the $\gamma^{\rm eff}$ represent actually the average result over this multidomain state.

Contrary to the case of 50 Oe, the fit results for 600 and 1500 Oe in both geometries are almost identical: We should change the values of $\gamma^{\rm eff}$, obtained by the fit of the data in L geometry for the $\gamma^{\rm eff} + 90^\circ$ (because $\gamma^{\rm eff}$ is determined in the coordinate system, connected with beam direction), and the calculations in T geometry give the acceptable result as well. That means that at these magnitudes of the external field (the bottom row in Fig. 14) we most probably have the single-domain state, and the obtained $\gamma^{\rm eff}$ presents the real layer-by-layer magnetization directions.

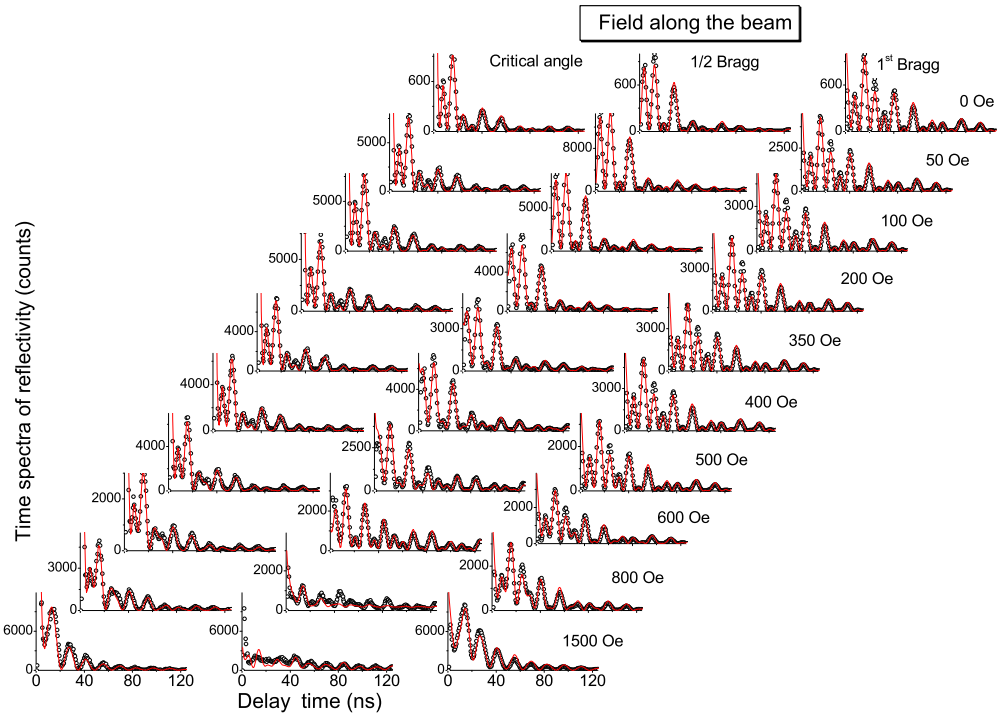

FIG. 12. (Color online) Time spectra of NRR reflectivity, measured at three incidence angles of SR for different magnitude of the ascending external field in L geometry. Symbols represent the experimental data, lines—the fit results.

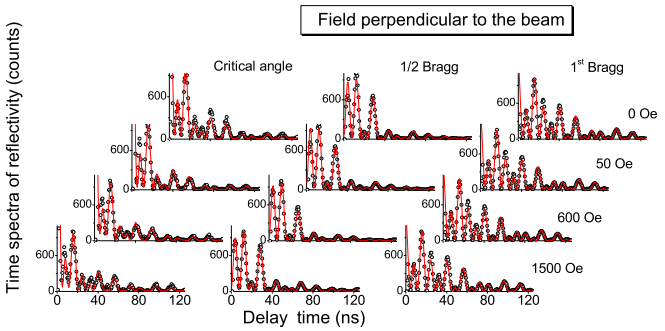

FIG. 13. (Color online) The same as in Fig. 12, but for T geometry.

At 600 Oe in T geometry we have observed the very high half-order Bragg peak and in qualitative consideration we have supposed that in such a way the "bulk" spin-flop effect manifests itself. The quantitative treatment of the data shows a noncollinear canted state. However, even such $\sim 140^\circ$ difference in magnetization directions for two magnetic sublattices (excluding bottom layers) is enough to create the high half-order Bragg peak contrary to the $(\gamma_1^{\text{eff}} + 90^\circ)/(\gamma_2^{\text{eff}} + 90^\circ) = 110^\circ/70^\circ$ at zero external field, because in the latter case it is not the real magnetization directions but the consequence of the partially coherent average of the scattering by different domains. We get the broadening of the angle between the magnetizations in the sublattices with external field increase getting the maximum at 350 Oe. That can be the evidence that the magnetizations in the two sublattices really try to line up perpendicular to the external field at this field. But we have no delayed reflectivity curve in T geometry at such field, so we are not sure that the data at this magnitude of the field are completely stipulated by the real magnetization directions but not by the partial coherence of the beam.

At 1500 Oe the half-order Bragg peak is still presented in the T geometry, so at the highest applied field we still have

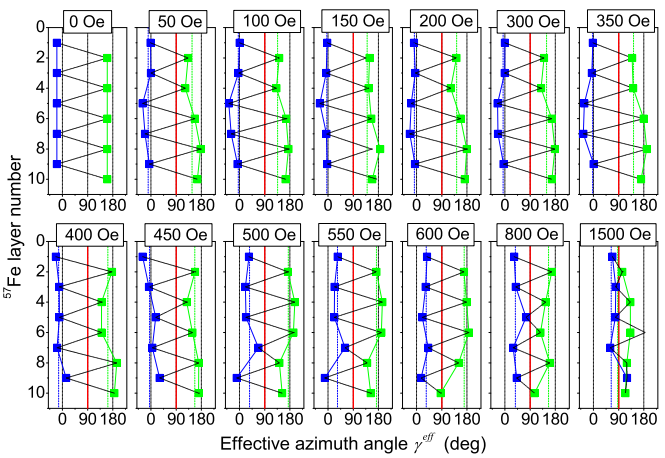

FIG. 14. (Color online) The layer-by-layer variations of the effective azimuth angle in our ML as a function of the ascending applied field; these are the results of the joint fit of the delayed reflectivity curves (Figs. 10 and 11) and time spectra of NRR reflectivity (Figs. 12 and 13).

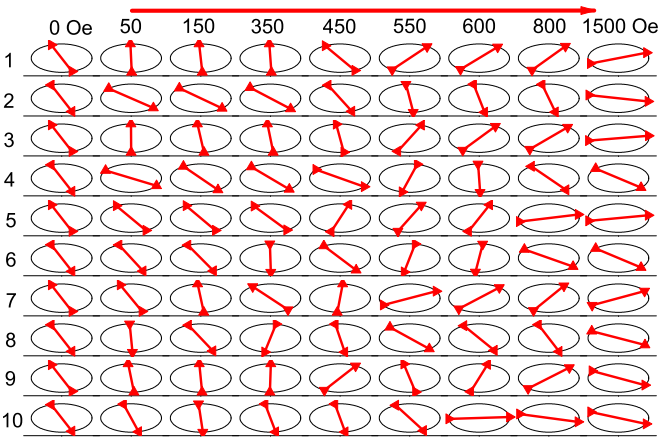

FIG. 15. (Color online) The same as in Fig. 14 (e.g., the magnetization directions in azimuth plane for ten ^{57}Fe layers of our ML) for the selected values of the external field, presented as polar graphs.

no total ferromagnetic alignment (as it could be concluded from the disappearance of the half-order Bragg peak in the L geometry). It is interesting that the relative intensities of the half-order Bragg peak and the first-order Bragg peak are almost the same at 0 and 1500 Oe. But the interpretation of these two dependencies is completely different. We believe that for 1500 Oe we get the real picture of the magnetization directions in Fig. 14, but at 0 Oe the specific azimuth angle of the antiferromagnetically coupled layers is the appearance of the partially coherent averaging of scattering from different magnetic domains.

The fit of the NRR data for our sample includes a huge amount of parameters (number of hyperfine parameters multiplied by the number of layers excluding the repetitions for the magnetization directions), so the problem of ambiguity of the presented picture in Fig. 14 is very serious. During the fit we have got sometimes the different models of magnetizations;

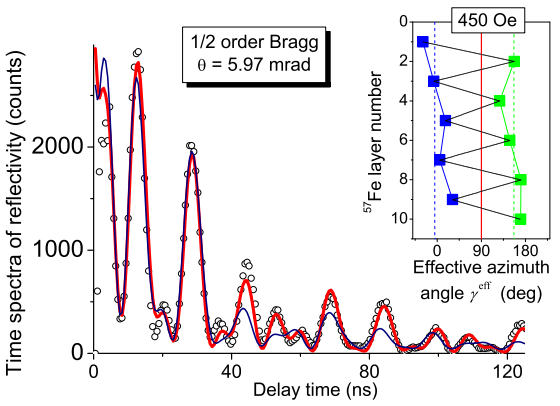

FIG. 16. (Color online) Time spectrum, measured at the half-order Bragg peak from our sample with 450-Oe field applied along the beam (symbols) and theoretical curves for two models (being results of the best fit of all the data for this field): for the model of collinear magnetization in two "magnetic sublattices"—5°/156.7°—(thin blue line) and the model of twisted magnetization (thick red line), presented in the inset (thin dashed vertical lines and lines with square symbols, respectively).

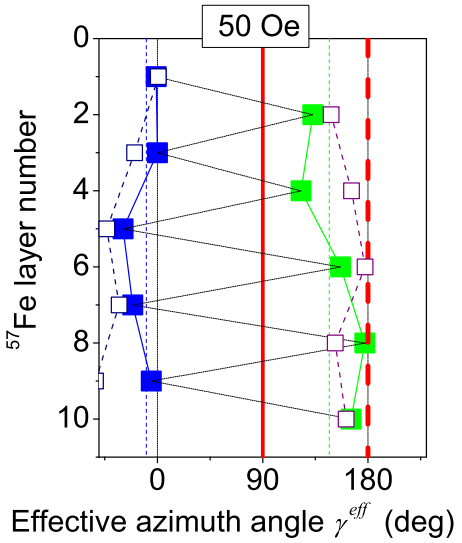

FIG. 17. (Color online) The layer-by-layer variations of the effective azimuth angle in our ML for the applied field of 50 Oe obtained from the fit of data for L geometry (filled squares) and T geometry (empty squares). The direction of the external field is drawn by a thick vertical line for the L geometry and by a thick dashed vertical line for the T geometry. Note that the effective azimuth angle γ^{eff} is determined in the axis, connected with beam direction (Fig. 1).

see Fig. 18. At first sight the obtained dependences presented by dashed (blue online) and solid (red online) lines give two completely different models. But we soon understood that actually they are the same. They differ just by the sign of the external field, but our experimental results are not sensitive to the sign of the magnetization (the method for overcoming this problem is described in, e.g., [38]). Therefore the observed two possible models just confirm that our fit is more or less reliable.

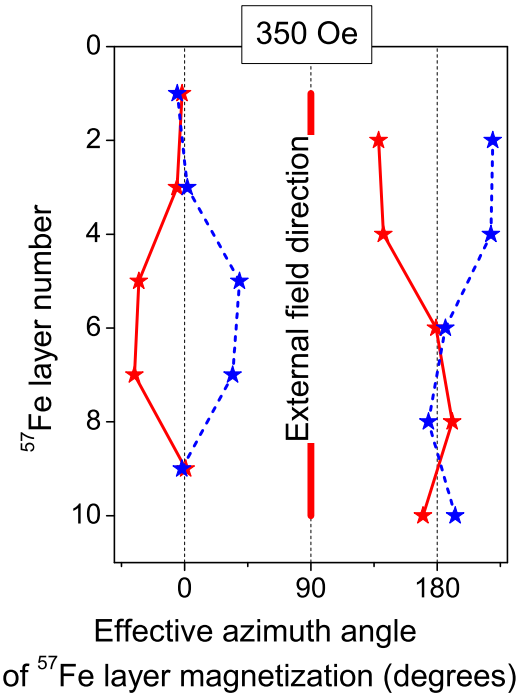

FIG. 18. (Color online) Two models of the depth profile of the ^{57}Fe layer magnetizations under the 350-Oe applied field obtained by the all-data joint fit.

We have not analyzed the inhomogeneous intralayer magnetic structure, mentioned hereinabove. Probably such consideration can slightly improve the fit results, but it essentially increases the number of the fit parameters and makes the task unsolvable. Besides, just the second-order Bragg peak is most sensitive to the interfaces (and their magnetization directions), but we have treated just the half- and first-order Bragg peaks for different values of the applied field.

VI. CONCLUSIONS

The obtained results, presented in Figs. 14 and 15, give a rather complicated picture of the layer-by-layer resolved reorientation of magnetization in ^{57}Fe layers under the applied field. The detailed analysis has shown that the collinear alignment in each magnetic sublattice and its cophasing rotation does not take place. We have seen that the reorientations even at the smallest applied field affected all layers, not just the top or bottom ones. The most specific magnetization state under the applied field is the twisted one, the bending details being the function of the applied field magnitude. The result should have some impact on the developing of the theory of the interlayer antiferromagnetic interaction. From our picture it is clear that in theory we cannot restrict ourselves by the interaction between just the adjacent magnetic layers, but should include the whole system simultaneously.

It may be noted that, in the case of multiparameter fitting of any experimental data, one can always doubt the uniqueness of the fitting. However, in the present case, in addition to the nuclear resonance specular reflectivity data we also have a set of the time spectra of the nuclear resonance reflectivity, taken at different angles of incidence, thus providing additional depth selectivity in measurements. This set of data is fitted simultaneously with the same values of parameters. Furthermore, measurements have been done as a function of applied magnetic field (ten different values of applied magnetic field, and two directions). For all these data, the parameters related to multilayer structure (e.g., layer thicknesses, roughnesses, hyperfine field of a layer) are kept the same. The only parameters which are varied from one set to the other are the directions of magnetization in different Fe layers. Thus we have a huge amount of data to fit a relatively smaller number of parameters. Thus the present situation is much better than that encountered in many of the excellent works in the literature (e.g., [6,11,16,17]).

In this study we take into account the influence on the real data interpretation of the partial coherence of the scattering from different domains. (Some modeling of such possible influence has been performed in [51].) We have shown that the azimuth angle which is used practically in all papers devoted to the magnetization depth profiles should be realized as the "effective azimuth angle." The real meaning of this angle depends on the ratio of the transverse coherence length of the used radiation relative to the average magnetic domain size.

ACKNOWLEDGMENTS

The work had been supported by The Russian Foundation for Basic Research (RFBR) Grants No. 09-02-01293-a, No. 13-02-00760-a, and No. 15-02-01502-a. Partial support through Science and Engineering Research Board (SERB) of India, Grant No. SB/S2/CMP-007/2013 is thankfully acknowledged. The synchrotron radiation experiments were performed at SPring-8 with the approval of the Japan Synchrotron Radiation Research Institute (JASRI) (Proposal No. 2010B1298). The authors are very grateful to the SPring-8 administration for hospitality and perfect conditions for the experiment realization.

[1] M. N. Baibich, J. M. Broto, A. Fert, F. Nguyen Van Dau, F. Petroff, P. Etienne, G. Creuzet, A. Friederich, and J. Chazelas, Phys. Rev. Lett. **61**, 2472 (1988).

[2] http://www.nobelprize.org/nobel_prizes/physics/laureates/2007/.

[3] V. V. Ustinov, M. A. Milayev, L. N. Romashev, T. P. Krinitsina, A. M. Burkhanov, V. V. Lauter-Pasyuk, and H. J. Lauter, J. Magn. Magn. Mater. **300**, e281 (2006).

[4] R. W. Wang, D. L. Mills, E. E. Fullerton, J. E. Mattson, and S. D. Bader, Phys. Rev. Lett. **72**, 920 (1994).

[5] J. W. Freeland, V. Chakarian, Y. U. Idzerda, S. Doherty, J. G. Zhu, H. Wende, and C. C. Kao, J. Vac. Sci. Technol. A **16**, 1355 (1998).

[6] V. Lauter-Pasyuk, H. J. Lauter, B. P. Toperverg, L. Romashev, and V. Ustinov, Phys. Rev. Lett. **89**, 167203 (2002).

[7] S. G. E. te Velthuis, J. S. Jiang, S. D. Bader, and G. P. Felcher, Phys. Rev. Lett. **89**, 127203 (2002).

[8] S. Rakhmanova, D. L. Mills, and E. E. Fullerton, Phys. Rev. B **57**, 476 (1998).

[9] L. Trallori, Phys. Rev. B **57**, 5923 (1998).

[10] N. Papanicolaou, J. Phys. Condens. Matter **10**, L131 (1998); **11**, 59 (1999).

[11] J. Meersschaut, C. L'abbé, F. M. Almeida, J. S. Jiang, J. Pearson, U. Welp, M. Gierlings, H. Maletta, and S. D. Bader, Phys. Rev. B **73**, 144428 (2006).

[12] V. V. Ustinov, N. G. Bebenin, L. N. Romashev, V. I. Minin, M. A. Milyaev, A. R. Del, and A. V. Semerikov, Phys. Rev. B **54**, 15958 (1996).

[13] A. I. Morosov and A. S. Sigov, Usp. Fiz. Nauk **180**, 709 (2010).

[14] V. V. Ustinov, http://www.imp.uran.ru/UserFiles/File/Dostizhenia/Ustinov.pdf.

[15] A. Nefedov, J. Grabis, and H. Zabel, Physica B **357**, 22 (2005).

[16] T. Diederich, S. Couet, and R. Röhlsberger, Phys. Rev. B **76**, 054401 (2007).

[17] S. Couet, K. Schlage, Th. Diederich, R Rüffer, K. Theis-Bröhl, B. P. Toperverg, K. Zhernenkov, H. Zabel, and R. Röhlsberger, New J. Phys. **11**, 013038 (2009).

[18] G. V. Smirnov, U. van Bürck, A. I. Chumakov, A. Q. R. Baron, and R. Rüffer, Phys. Rev. B **55**, 5811 (1997).

[19] T. Mitsui, N. Hirao, Y. Ohishi, R. Masuda, Y. Nakamura, H. Enoki, K. Sakaki, and M. Seto, J. Synchrotron Radiat. **16**, 723 (2009).

[20] V. Potapkin, A. I. Chumakov, G. V. Smirnov, J.-Ph. Celse, R. Rüffer, C. McCammon, and L. Dubrovinsky, J. Synchrotron Radiat. **19**, 559 (2012).

[21] G. V. Smirnov, Hyperfine Interact. **123/124**, 31 (1999).

[22] A. I. Chumakov, L. Niesen, D. L. Nagy, and E. E. Alp, Hyperfine Interact. **123/124**, 427 (1999).

[23] M. A. Andreeva and B. Lindgren, Phys. Rev. B **72**, 125422 (2005).

[24] M. A. Andreeva, N. G. Monina, S. Stankov, Moscow Univ. Phys. Bull. **63**, 132 (2008).

[25] http://www.esrf.eu/computing/scientific/REFTIM/MAIN.htm.

[26] M.A. Andreeva, Hyperfine Interact. **185**, 17 (2008).

[27] See Supplemental Material at http://link.aps.org/supplemental/10.1103/PhysRevB.92.134403 for the general theory of the nuclear resonance reflectivity.

[28] R. Azzam and N. Bashara, *Ellipsometry and Polarized Light* (North-Holland P.C., Amsterdam, 1977).

[29] G. N. Borzdov, L. M. Barkovskii, and V. I. Lavrukovich, J. Appl. Spectrosc. **25**, 1174 (1976).

[30] M. A. Andreeva and K. Rosete, Vestn. Moscovskogo Univ., Fiz. **41**, 65 (1986) (English transl. by Allerton press, Inc.).

[31] M. A. Andreeva and K. Rosete, Poverkhnost' **9**, 145 (1986) (In Russian).

[32] S. M. Irkaev, M. A. Andreeva, V. G. Semenov, G. N. Belozerskii, and O. V. Grishin, Nucl. Instrum. Methods Phys. Res., Sect. B **74**, 554 (1993).

[33] I. W. Hamley and J. S. Pedersen, J. Appl. Crystallogr. **27**, 29 (1994).

[34] M. A. Andreeva and Yu. L. Repchenko, Crystallogr. Rep. **58**, 1037 (2013).

[35] M. Blum and O. C. Kistner, Phys. Rev. **171**, 417 (1968).

[36] D. L. Nagy, L. Bottyán, L. Deák, B. Degroote, J. Dekoster, O. Leupold, M. Major, J. Meersschaut, R. Rüffer, E. Szilágyi, and A. Vantomme, Hyperfine Interact. **141/142**, 459 (2002).

[37] M. A. Andreeva, V. G. Semenov, L. Häggström, B. Kalska, B. Lindgren, A. I. Chumakov, O. Leupold, and R. Rüffer, Hyperfine Interact. **136/137**, 687 (2001).

[38] C. L'abbé, J. Meersschaut, W. Sturhahn, J. S. Jiang, T. S. Toellner, E. E. Alp, and S. D. Bader, Phys. Rev. Lett. **93**, 037201 (2004).

[39] T. Ślęzak, M. Ślęzak, M. Zając, K. Freindl, A. Kozioł-Rachwał, K. Matlak, N. Spiridis, D. Wilgocka-Ślęzak, E. Partyka-Jankowska, M. Rennhofer, A. I. Chumakov, S. Stankov, R. Rüffer, and J. Korecki, Phys. Rev. Lett. **105**, 027206 (2010).

[40] J. Stöhr, H. A. Padmore, S. Anders, T. Stammler, and M. R. Scheinfein, Surf. Rev. Lett. **05**, 1297 (1998).

[41] F. Nolting, A. Scholl, J. Stöhr, J. W. Seo, J. Fompeyrine, H. Siegwart, J.-P. Locquet, S. Anders, J. Lüning, E. E. Fullerton, M. F. Toney, M. R. Scheinfeink, and H. A. Padmore, Nature **405**, 767 (2000).

[42] W. Kuch, X. Gao, and J. Kirschner, Phys. Rev. B **65**, 064406 (2002).

[43] R. Röhlsberger, J. Bansmann, V. Senz, K. L. Jonas, A. Bettac, K. H. Meiwes-Broer, and O. Leupold, Phys. Rev. B **67**, 245412 (2003).

[44] R. Röhlsberger, *Nuclear Condensed Matter Physics with Synchrotron Radiation, Basic Principles, Methodology, and Applications*, Springer Tracts in Modern Physics Vol. 208 (Springer, Berlin, 2004).
[45] M. A. Andreeva, N. G. Monina, B. Lindgren, L. Häggström, and B. Kalska, JETP **104**, 577 (2007).
[46] A. Q. R. Baron, A. I. Chumakov, H. F. Grünsteudel, H. Grünsteudel, L. Niesen, and R. Rüffer, Phys. Rev. Lett. **77**, 4808 (1996).
[47] A. Q. L. Baron, Hyperfine Interact. **123/124**, 667 (1999).
[48] Y. V. Shvyd'ko, A. I. Chumakov, A. Q. R. Baron, E. Gerdau, R. Rüffer, A. Bernhard, and J. Metge, Phys. Rev. B **54**, 14942 (1996).
[49] L. Bottyán, J. Dekoster, L. Deák, B. Degroote, E. Kunnen, C. L'abbé, G. Langoucher, O. Leupold, M. Major, J. Meersschaut, D. L. Nagy, and R. Rüffer, in *ESRF Highlights* (1999), Ed. by European Synchrotron Radiation Facility, p. 62, http://www.esrf.eu/UsersAndScience/Publications/Highlights.
[50] R. M. Osgood III, S. K. Sinha, J. W. Freeland, Y. U. Idzerda, and S. D. Bader, J. Magn. Magn. Mater. **198–199**, 698 (1999).
[51] L. Deák, L. Bottyán, D. L. Nagy, H. Spiering, Yu. N. Khaidukov, and Y. Yoda, Phys. Rev. B **76**, 224420 (2007).
[52] E. Kravtsov, D. Haskel, S. G. E. te Velthuis, J. S. Jiang, and B. J. Kirby, Phys. Rev. B **79**, 134438 (2009).
[53] P. Sharma and A. Gupta, Nucl. Instrum. Methods Phys. Res., Sect. B **244**, 105 (2006).